Military Technical College
Kobry El-Kobbah,
Cairo, Egypt.

17th International Conference on Applied Mechanics and Mechanical Engineering.

OPTIMIZATION OF ELECTRON BEAM WELDING PARAMETERS OF DISSIMILAR JOINT OF AISI 304 STAINLESS STEEL AND AISI 1020 LOW CARBON STEEL

M. Nasr El-Deen*,[1], M. E. Shamekh*, W. Elthalabawy* and M.T. Sallam*

ABSTRACT

This paper presents the optimization of welding parameters of electron beam welded joint of dissimilar materials namely AISI 304 stainless steel and AISI 1020 low carbon steel (0.21% C.). Three main welding parameters were investigated. These parameters are welding current, focusing current, and welding speed. The optimization was based, from one hand, on microstructure analysis of both bead and heat affected zones, using optical and scanning electron microscopes, and, from the other hand, the evaluation of tensile, impact, and micro-hardness mechanical properties. The results of the investigation showed that, an optimum welding current of 19 mA, a focusing current of 875 mA, and a welding speed of 8mm/s at a working distance 100 mm can provide uniform welding bead with full penetration, without undercuts and a narrow width of HAZ in the order of 2.3 mm. Moreover, they can secure a tensile failure outside the joint, in the base metal (low carbon steel) satisfying a tensile strength of about 430 MPa. Furthermore, the impact resistance of the joint was found to provide about 160 J/cm^2 (hummer against the root of bead) and about 70 J/cm^2 (hummer against the face of bead). The hardness distribution along the joint from the stainless steel side to the low carbon steel side through the bead and HAZ was determined, and indicates that, a maximum hardness of about 380 HV was obtained in the center of the bead. This value is higher than the obtained hardness values of both the austenitic stainless steel and low carbon steel.

KEYWORDS

HAZ: Heat Affected Zone, **EBW:** Electron Beam Welding

* Egyptian Armed Forces.
[1] Email of corresponding author (meromoro50@gmail.com)

INTRODUCTION

Several situations in industrial practice face challenges which call for joining of dissimilar materials [1,2]. The joining of dissimilar metals is generally more complex than that of similar metals because of the difference in the physical, mechanical, and metallurgical properties of both parent metals to be joined [3,4]. Aerospace vehicles and nuclear reactors are examples of the most important applications among many others. In nuclear water reactors, dissimilar metal welds are employed to connect the low alloy steel reactor pressure vessel and stainless steel pipe systems [1,3,5].

The problem with the dissimilar metal weld made between low alloy steel and austenitic stainless steel is the carbide formation due to higher carbon content of low alloy steels than that of austenitic stainless steel [6,7]. Many techniques used to weld dissimilar metals such as shielded metal arc welding, gas metal arc welding, tungsten arc welding, plasma arc welding [3,4,5], laser beam welding, and electron beam welding[3,8].

Due to these critical applications, electron beam welding technique is used. In electron beam welding, the heat input is concentrated on the interface and melts the metal (Keyhole phenomena) [8]. Many parameters control this process like welding current, focusing current, welding speed, sweep size, and working distance between the gun and work piece. [8,9].

N. Arivazhagan, studied the investigation on 304 austenitic stainless steel to 4140 low alloy steel dissimilar joints by gas tungsten arc, friction welding, and electron beam welding. The analysis showed that the joint made by EBW has the highest tensile strength than the joint made by GTAW and FRW. He also found that the ductility of the EBW and GTA weldment were higher compared with friction weldment [10].

I. Hajiannia,[11], Investigated the microstructure and mechanical properties of AISI 347 austenitic stainless steel to ASTM A335 low alloy steel dissimilar joint by using TIG with two filler metals including ER309L and ERNiCr-3. The tensile test analysis showed that all weldments failed in the HAZ of A335 low alloy steel.

ZHANG Bing-gang, [12], studied the temperature and stress fields in electron beam welded Ti-15-3 alloy to 304 stainless steel joint with copper interlayer sheet. He concluded that the temperature distribution is asymmetric along the weld center and the temperature in the titanium alloy plate is higher than that in the 304 STS plate.

In this paper, three major electron beam welding parameters were optimized and investigated. These parameters control the magnitude of the heat input delivered to the joint during the welding process [13,14,]. The optimization of these parameters was based on the evaluation of the obtained microstructure and mechanical properties [15].

EXPERIMENTAL WORK

The base metals employed in this study are austenitic stainless steel (AISI 304) and

low carbon steel (AISI 1020). These base metals were both delivered in the form of rolled plates 5 mm thickness. Composition analysis had been determined by using X-Ray florescence and Spark emission spectroscopy. The chemical compositions of both metals are shown in Table 1.

Table 1. Chemical composition of base metals.

	C%	Mn%	Si%	Cr%	Ni%	Cu%	P%	S%	Fe%
AISI 304	0.08	2.00	1.00	18.5	8.75	0.045	<0.035	<0.030	balance
AISI 1020	0.21	0.45	0.25	0.019	0.025	0.013	<0.040	<0.050	balance

The metals were cut into similar plates with dimensions 100x80x5 mm by using laser machine model (TruLaser 3030) as shown in Fig.1

Fig. 1. The Laser Machine type (TruLaser 3030) used in cutting plates and test specimens.

Several different plates were welded by electron beam welding technique without edge preparation and air gap under constant accelerating voltage of 60 KV, vacuum pressure of $26x10^{-3}$ Pa and working distance of 100 mm, using an EBW machine model (SeoTECH-60) shown in Fig. 2.

Three major welding parameters were chosen to be investigated, and each has been varied independently while keeping the other parameters to be constant. Welding current, as a welding parameter, has the major effect on the value of the energy input and the resulting characteristic of the welded joint. This welding current was changed during this investigation from 9 mA up to 29 mA. Outside these range, joining was difficult to take place. On the other hand, the focusing current, which is considered as

Fig. 2. The Chamber of the used Electron Beam Welding Machine.

the second basic welding parameter, having a notable effect on controlling the position of the beam spot along the thickness of the plate, concentrates the input energy in the vertical position. By increasing the focusing current, thebeam spot shifts down from the surface, through the thickness, to the root of the joint. Focusing current was varied from 865 mA to 885 mA to secure the required depth of beam spot. The welding speed, which also considerably affects the value of the energy input, during the weld, was varied from 3mm/s up to 13mm/s. A working distance of 100 mm was kept constant during carrying out of all experimental joints.

Standard tensile test specimens, having the welded bead, in the middle, perpendicular to the longitudinal axis of the specimen, were cut from the welded plates according to ASTM E8. These specimens have a gauge length of 80 mm and a gauge area of 20x5mm. Tensile test was carried out on these specimens according to ASTM E8/E8M-13 under strain rate of 10^{-3} s^{-1}, using a universal tensile electro-hydraulic testing machine type Instron 8032.

Furthermore, non-standardize non-notched impact specimens having dimensions 55x10x5mm were also cut, so that, the weld bead is located in the middle of the specimen length. Impact test was carried out, on each specimen, in two directions, hummer against face and hummer against root of the weld, by using automatic impact testing machine type Galdabini 300.

Hardness test, was carried out, applying the Vicker's hardness test method, according to ISO 17025, using Zwick hardness tester applying indentation load of 1 Kg. HV values were recorded along a line perpendicular to the weld bead from the side of the austenitic stainless steel through HAZ and bead toward the low carbon steel side.

Specimens for microstructure were prepared applying the standard procedure, after mounting in polyethylene holders, grinding with emery papers of varies grades 180, 250, 400, 600, 800, and 1200,was carried out, followed by polishing using an emulsion of AL_2O_3 in distilled water, to have a mirror like surface. Revealing of the

structure was carried out using two types of etchants, due to the different sensitivity of reaction of both structures for a single etchant. Etching was first applied by immersion in Nital reagent (3% NHO_3 - methyl alcohol) for 10s to reveal the low carbon steel structure. Afterward, Villa's etchant (5cc HCL + 2gr Picric acid + 100cc Ethyl alcohol) was applied for 1 min. to reveal the austenitic and bead structure. Low carbon steel structure after applying this second etchant was severely over etched and becomes extremely dark. The different microstructures were examined by an optical microscope type Olympus BX41M.

The tensile fracture of test specimens was investigated to determine the different modes and mechanisms of failure using scanning electron microscope type Remma 202 under an accelerating voltage of 30 KV.

RESULTS AND DISCUSSIONS

Microstructure Analysis

The obtained microstructures of the base metals are illustrated in Fig.3. The structure of the AISI 304 stainless steel Fig.3a demonstrates clear austenitic phase having relatively coarse elongated grains with occasional twinning. On the contrary, the structure of the low carbon steel AISI 1020 Fig.3b reveals a mixture of pearlite and a dominant ferritic phase. We can note also the deformation and elongation of the grains in the direction of the previous rolling operations.

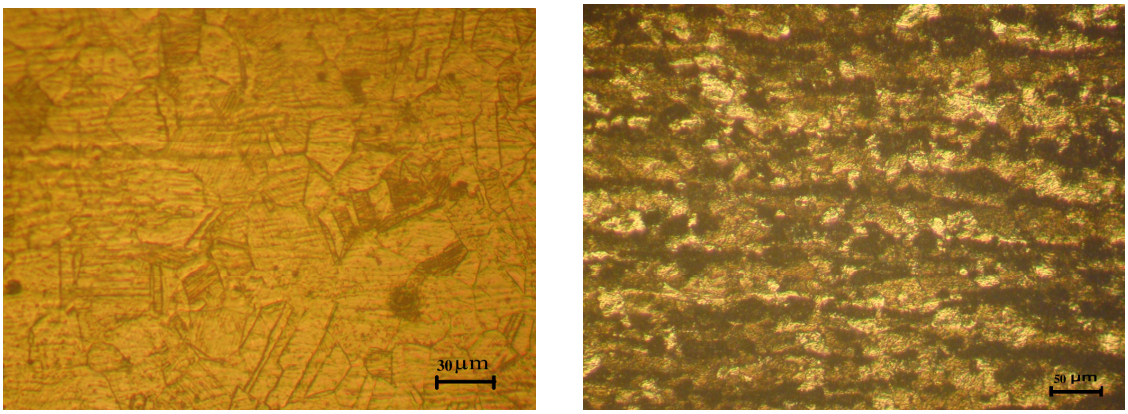

a) AISI 304 Stainless Steel b) Low Carbon steel AISI

Fig.3. Microstructures of base metals a) AISI 304 Austenitic stainless steel b) AISI 1020 Low Carbon steel.

The evolution of the structure from the bead towards the base metal through the transition boundary and heat affected zone (HAZ), of dissimilar welded joint between the adopted austenitic stainless steel and low carbon steel, is demonstrated in Fig.4. This joint was elaborated by applying a welding current of I_w=9mA, focusing current of I_f=875mA, and a welding speed of v=8mm/s. The bead clarified a dense fine dendrites perpendicular to the transition boundary, on both sides. On the other hand, we can note a sensible coarsening of grains in the zone adjacent to the transition boundary between bead and HAZ, which was not subjected to melting but exposed

to a relatively high temperature as shown in Fig.5a. The temperature decreases gradually through HAZ towards the base metal, in a monotonic way, which results in less coarse grains. The structure at a distance 4.3 mm from the center of the bead, which demonstrates a deformed elongated grain structure, as shown in Fig.5b, indicates that this zone is not affected by the heat and, consequently, it marks the width of the HAZ and its boundary with the base metal.

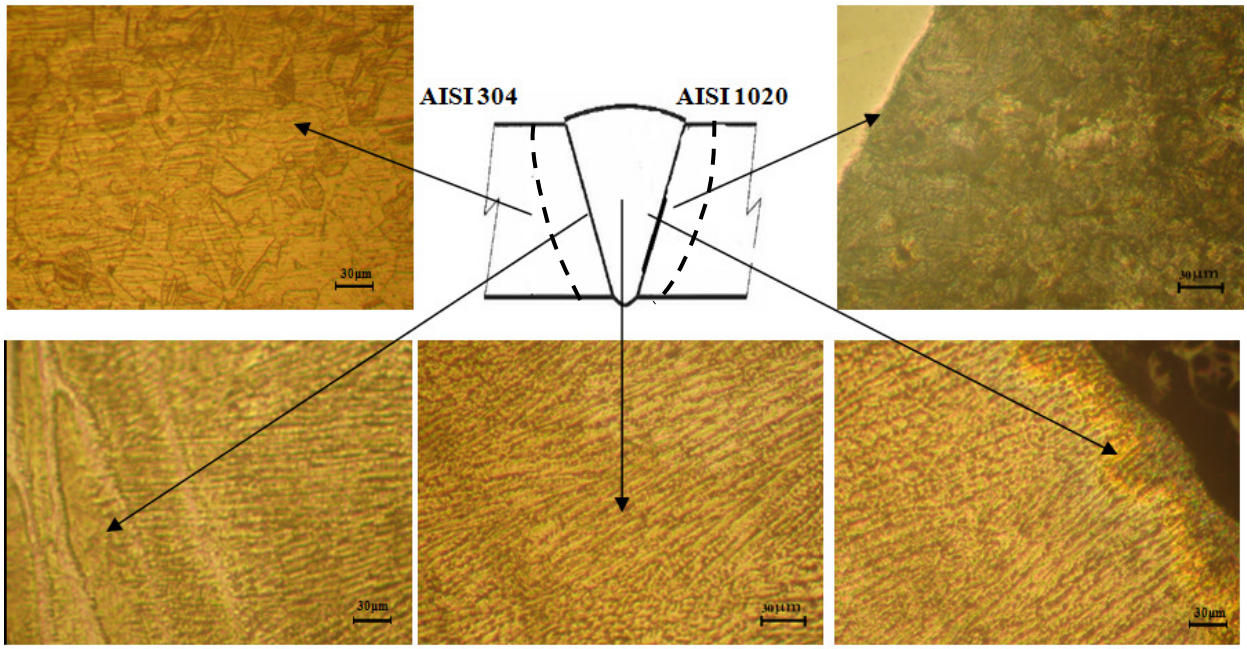

Fig 4. Microstructure of dissimilar welded joint of AISI 304 and AISI 1020 with I_w=9 mA, I_f=875 mA and v=8mm/s, at different zones.

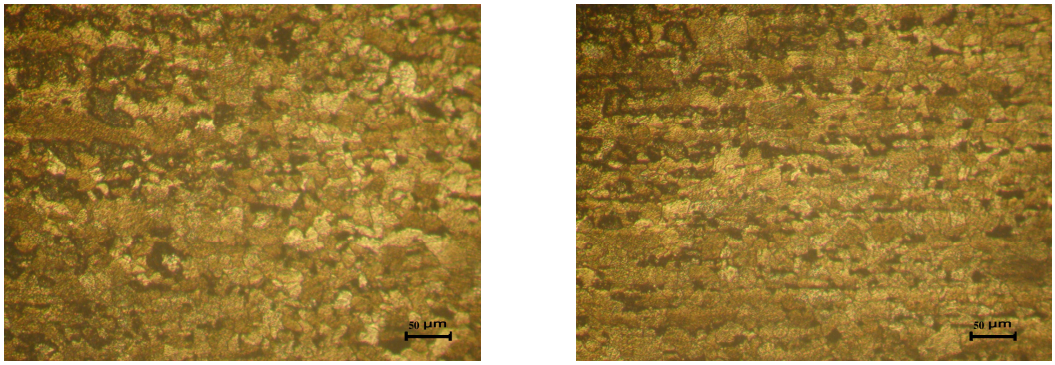

a) **b)**

Fig.5. Microstructures of the joint side of Low Carbon steel AISI 1020; a) In the HAZ adjacent to the transition boundary b) Away from HAZ on the base metal.

Figure 6 elucidates the effect of increasing, only the welding current to I_w=19 mA, for the same joint, and keeping all the other parameters constant, on the structure of the bead and HAZ. We can clearly note that the structure of these zones is coarser than the joint welded with a welding current I_w=9 mA. In fact, welding current is considered a predominant welding parameter controlling the heat input to the welded joint and consequently the obtained structure after solidification of the bead and cooling of the joint.

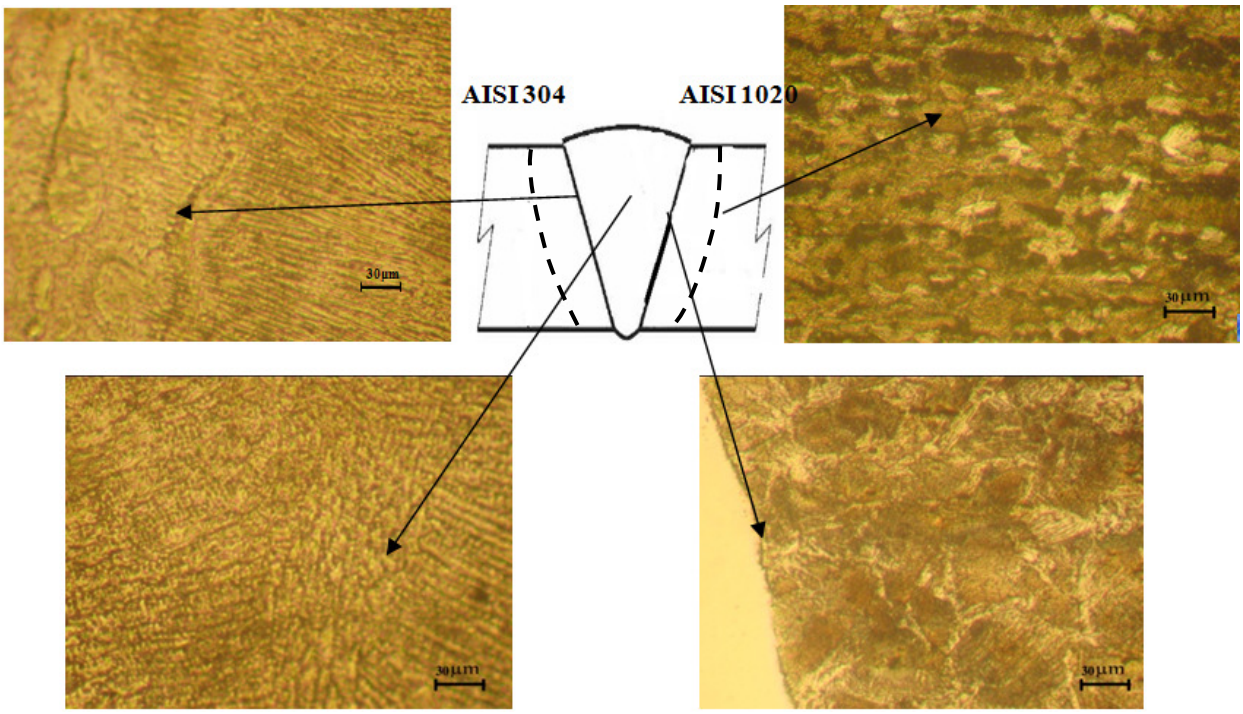

Fig 6. Microstructure of dissimilar welded joint of AISI 304 and AISI 1020 with I_w=19 mA, I_f=875 mA and v=8mm/s, at different zones.

Mechanical Results

Figure 7 illustrates typical Stress-Strain curves obtained during testing welded dissimilar joints of austenitic stainless steel and low carbon steel, by different welding current I_w with constant focusing current of I_f=875 mA and welding speed of v=8mm/s. When a welding current of 9 mA was applied, the maximum ultimate tensile strength obtained was on the order of 261MPa while the ductility calculated was in the order of (2%). Increasing the welding current to 14 mA, results in an increase of both ultimate tensile strength and ductility. Maximum values of these characteristics (σ_u= 430 MPa and δ%= 12.5) were achieved when the welding current was increased to 19 mA. We can note that when I_w was increased from 9 to 19mA, a corresponding increase of ultimate tensile strength of 65% and ductility of 525% were obtained. Furthermore, increasing the welding current above 19 mA drives to lower values of both ultimate strength and ductility. The application of low welding current does not secure the proper value of heat input which can provide full penetration, proper melting of edges, and uniform molten bead. Moreover, relatively, high welding currents over heat the joint, increase its temperature and results in coarser structure and non uniform bead waving and over penetration. These effects seriously influence the mechanical characteristics of the formed joint.

Figure 8 shows the variation of the ultimate tensile strength obtained during tensile tests carried out on the dissimilar joints of austenitic stainless steel and low carbon steel as a function of welding current keeping all the other parameters constant. This figure clearly visualize that the maximum and the optimum welding current is in the order of 19 mA.

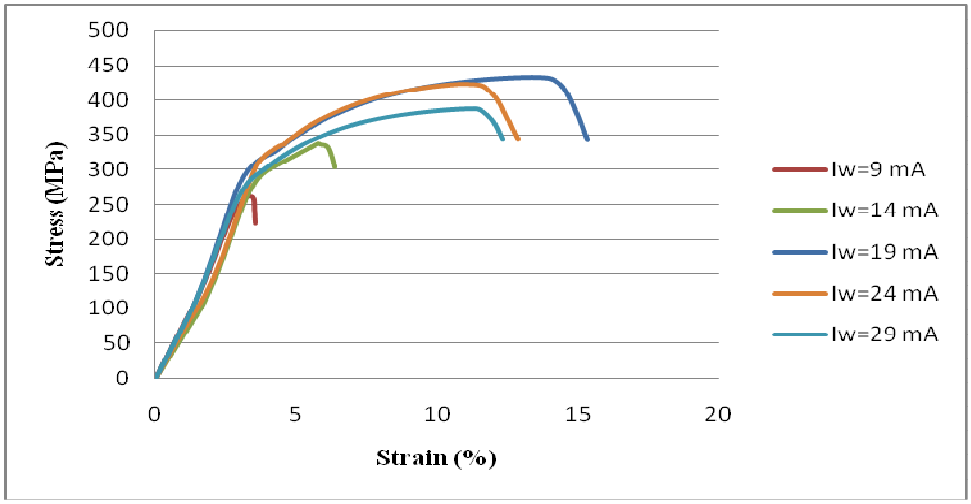

Fig. 7. Typical Stress-Strain curves obtained during testing welded dissimilar joints of austenitic stainless steel and low carbon steel, by different I_w with constant I_f=875 mA and v=8mm/s.

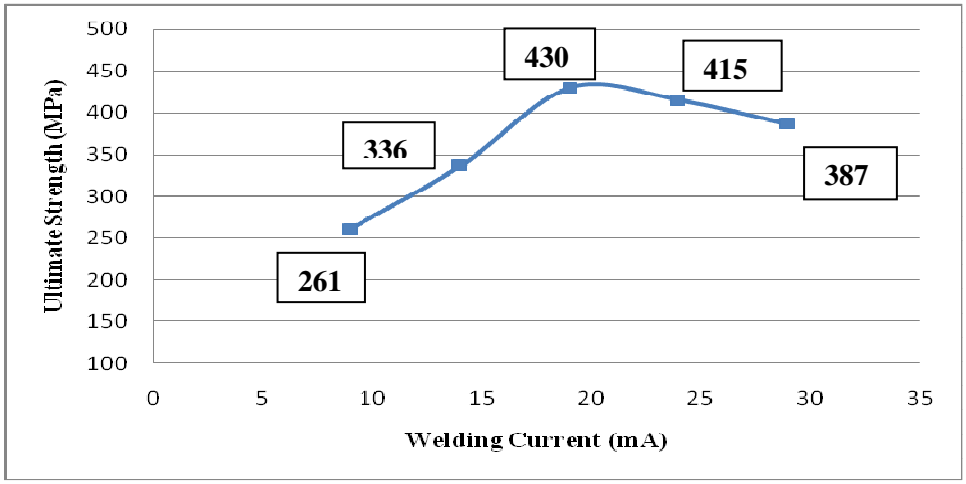

Fig. 8. The variation of the ultimate tensile strength obtained during tensile tests carried out on the dissimilar joints of AISI 304 austenitic stainless steel and AISI 1020 low carbon steel.

Figure 9, which demonstrates the variation of the measure ductility of the indicated joints as a function of welding current, confirms that the revealed value of welding current is optimum for both strength and ductility.

Figure 10 shows the variation of the characteristics of typical stress-strain curve, of welded dissimilar joints of austenitic stainless steel and low carbon steel by changing the welding speed, at an optimum welding current of I_w=19 mA and focusing current of I_f=875 mA. It can be noted that, by increasing the welding speed up to 8 mm/s, the ultimate tensile strength increases. For higher welding speeds, the ultimate tensile strength decreases as summarized in Fig.11. On the other hand, the ductility showed a monotonic decrease with increasing the welding speed as illustrated in Fig.12. These influences of welding speed on ultimate tensile strength and ductility can be attributed to the complex combined effects of different coefficients of thermal

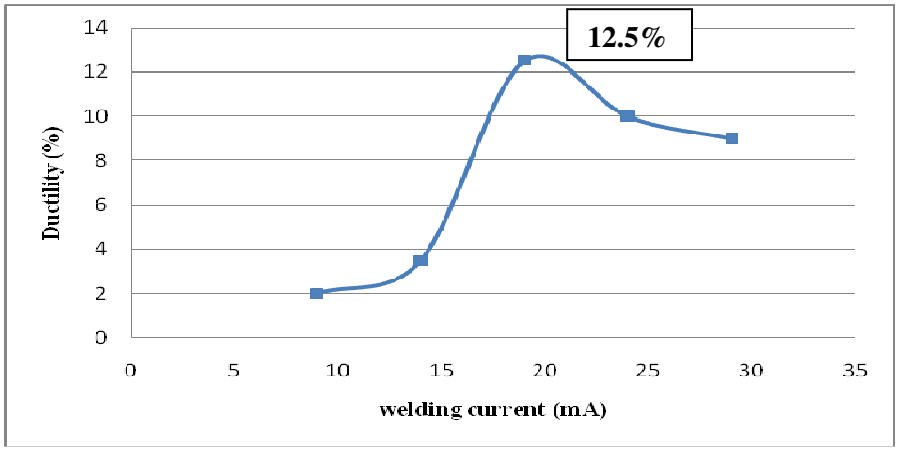

Fig. 9. The Variation of the ductility obtained during tensile tests carried out on the dissimilar joints of AISI 304 austenitic stainless steel and AISI 1020 low carbon steel.

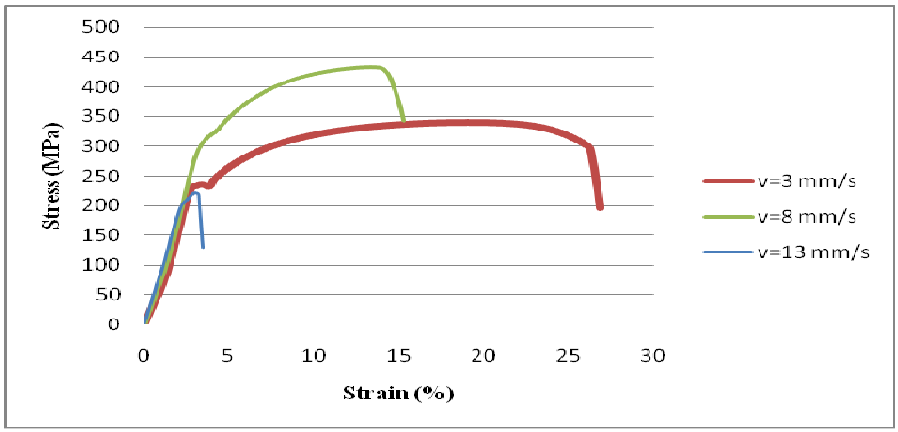

Fig. 10. Typical Stress-Strain curves obtained during testing welded dissimilar joints of austenitic stainless steel and low carbon steel, by different welding speed with constant I_w=19 mA and I_f=875 mA.

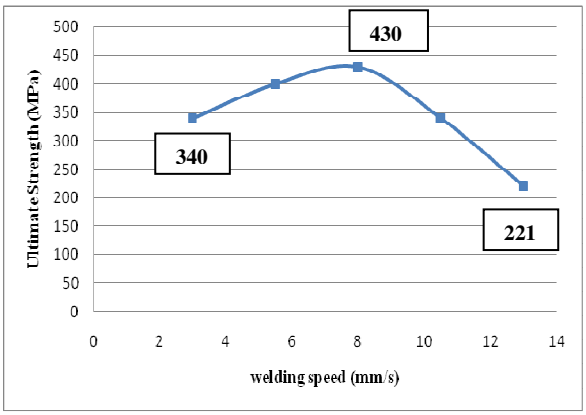

Fig. 11. The variation of the ultimate tensile strength against welding speed

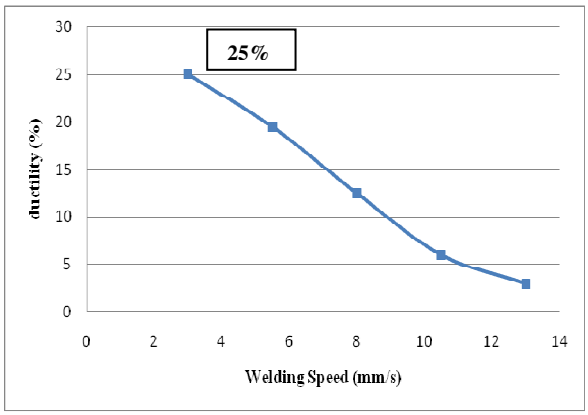

Fig. 12. The variation of the ductility of the joint against welding speed

expansion, different coefficients of thermal conductivity, different coefficients of diffusion, and different compositions [16,17]. The optimum value of welding speed is correlated to the applications and requirements on the elaborated joint. When strength is the major target, then a welding speed of 8mm/s can provide an optimum value, while, when ductility is of prime importance, then the low value of welding speed v=3mm/s can establish an optimum value.

Figure 13 presents the effect of changing the focusing current on the resulting stress-strain curves of dissimilar joints of austenitic stainless steel and low carbon steel under a constant welding current of I_w= 19 mA and a welding speed of v= 8 mm/s. The investigation of the effect of the focusing current, which controls the position of the electron beam spot through the thickness of the specimen from the top surface to the bottom root, showed a similar behavior of the obtained mechanical properties as those measured during varying the welding speed. By increasing the focusing current, ultimate tensile strength increases up to a maximum value of 430 MPa at a focusing current of 875 mA where further increase of the focusing current leads to decrease this strength, as shown in Fig.14. Moreover, by increasing the focusing current, the ductility monotonically decreases, as illustrated in Fig.15. The optimum value of the focusing current can also be determined on the same bases as welding speed.

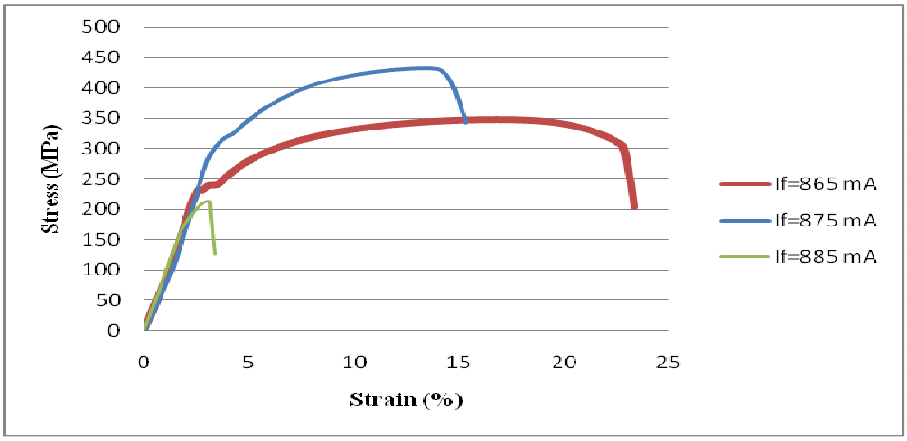

Fig. 13. Typical Stress-Strain curves obtained during testing welded dissimilar joints of austenitic stainless steel and low carbon steel, by different focusing current with constant I_w=19 mA and v=8 mm/s.

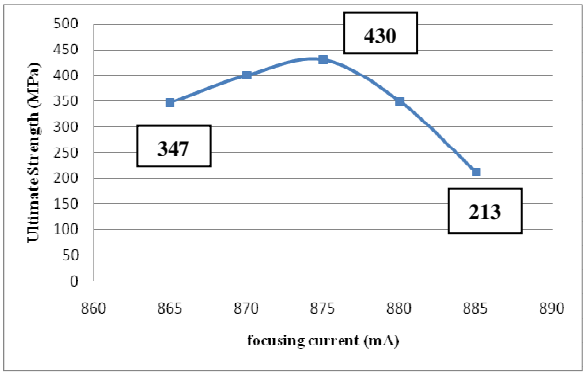

Fig. 14. The variation of the ultimate tensile strength against focusing current.

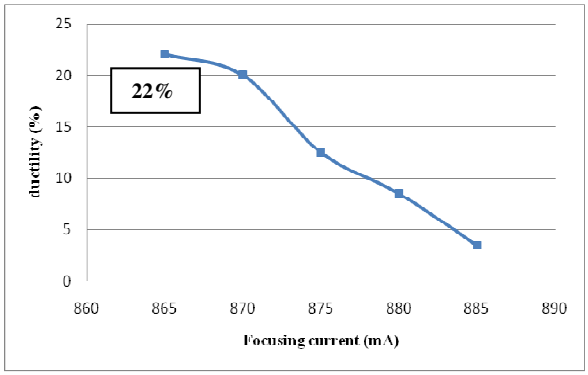

Fig. 15. The variation of the ductility of the joint against focusing current.

Figure 16 illustrates the Tensile fracture surface, obtained outside the welded bead, in the base metal of AISI 1020 low carbon steel, after testing a dissimilar welded joint of austenitic stainless steel and low carbon steel, using welding parameters I_w=19 mA, I_f=875 mA and v=8mm/s. We can note that, the fracture, in its totality, presents ductile modes taking place by dimples mechanism. On the other hand, we can remark the stretch and elongation of these dimples in the previous direction of plate deformation. This obtained fracture is exactly similar to that obtained after testing the fracture plates of the low carbon steel. When the welding current I_w was reduced to 9 mA, keeping the other parameters constant, on the same dissimilar joint, the quality of the joint was reduced, and incomplete penetration was manifested, consequently, the fracture took place in the bead. The fracture surface reveals, in addition to the ductile dimple modes, other brittle modes, which took place, either by cleavage, or intergranular fracture mechanisms. This can be attributed to, from one hand, the dendritic structure of the solidified bead, and from the other hand, the formation of the single and complex carbides, in this region, from both iron and chromium, due to concentration gradients, and diffusion process, as shown in Fig.17.

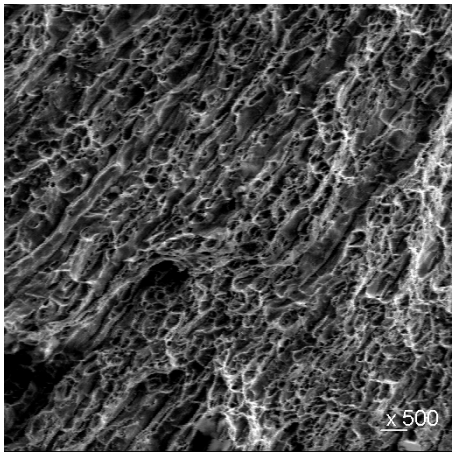

Fig.16. Tensile fracture surface, obtained outside the welded bead, in the base metal of AISI 1020 low carbon steel, after testing a dissimilar welded joint of austenitic stainless steel and low carbon steel, using welding parameters I_w=19 mA, I_f=875 mA and v=8mm/s.

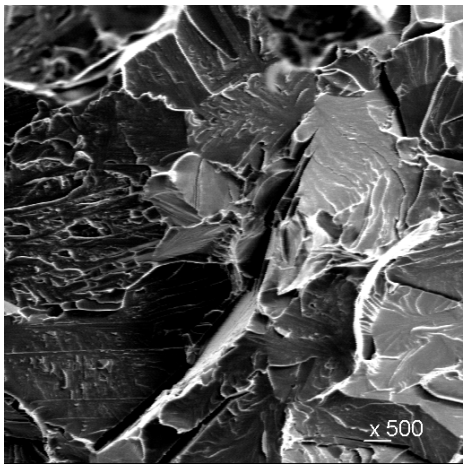

Fig.17. Tensile fracture surface, obtained in the welded bead, after testing a dissimilar welded joint of austenitic stainless steel and low carbon steel, using welding parameters I_w=9 mA, I_f=875 mA and v=8mm/s.

The results of the measured impact toughness on the electron beam dissimilar joints, of austenitic stainless steel and low carbon steel, as a function of welding current, under constant a focusing current of 875 mA and a welding speed of 8 mm/s, are demonstrated in Fig.18. The impact toughness was measured in two directions, hummer against the root of bead and hummer against the face of bead. When hummer strikes against the face of the bead, the root serves as a notch, in joints with partial or bad penetration. On the contrary, when hummer strikes against the root of the bead, the joint performs as non-notched impact specimen. This can explain the higher values of the impact toughness obtained when the hummer strikes against the root of the bead (non-notched impact specimen). On the other hand, a maximum values of impact toughness, in both directions of hummer strike relative to the bead, of about 79 J and 33.6 J respectively, at an optimum welding current I_w=19 mA.

The effects of welding speed and focusing current on impact toughness, keeping the other welding parameters constant, are illustrated in Fig.19. We can note that the determined optimum focusing current and welding speed from the analysis of the results of the tensile tests can also provide maximum values of impact toughness.

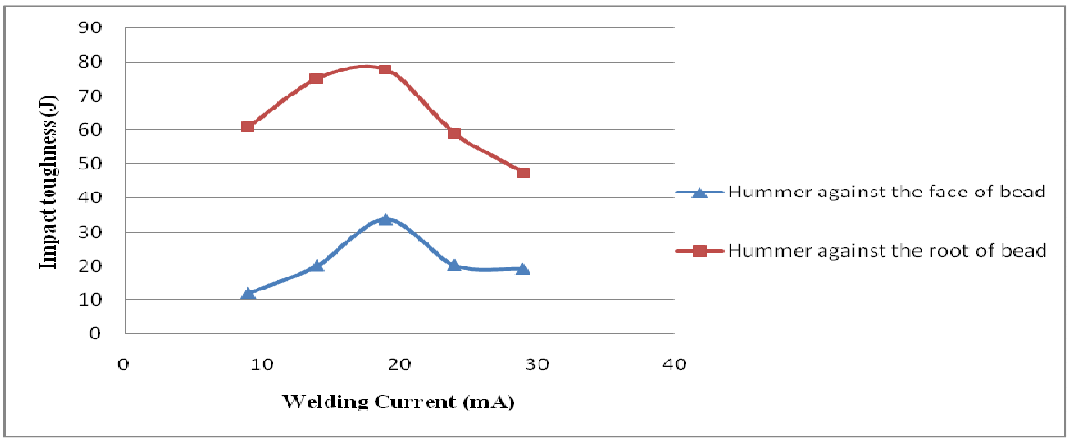

Fig. 18. The Effect of welding current on impact toughness, of welded dissimilar joints of austenitic stainless steel and low carbon steel, in the direction (hummer against the face of bead and in the opposite direction hummer against the root of bead) with constant I_f=875 mA and v=8 mm/s.

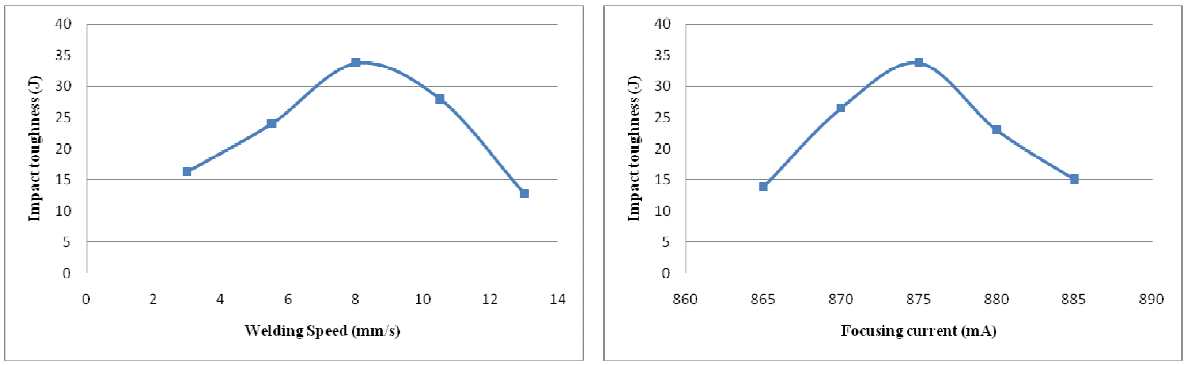

(a) **(b)**

Fig. 19. The effect of focusing current and welding speed on Impact Resistance, of welded dissimilar joints of austenitic stainless steel and low carbon steel at a constant optimum welding current of I_w=19mA.

Figure 20 shows the hardness distribution, along a line, from the stainless steel side of the welded plates, through the heat affected zones and formed bead, to the low carbon steel side of the joint. The measured values of hardness indicated that the initial plates hardness are in the order of 200 HV and 135 HV for AISI 304 stainless steel and AISI 1020 low carbon steel respectively. This difference in hardness is clearly explained by the composition of the austenitic stainless steel which contains 18.5% Cr. and 8.75% Ni, mostly in its solution. Moreover, a peak of hardness of 380 HV was obtained in the center of the bead, which can be attributed to the diffusion of chromium from the austenitic stainless steel towards the low carbon steel side and the reverse diffusion of carbon in the opposite direction, according to the established concentration gradients between the different elements in the two plates. The occurrence of these diffusion processes, throughout welding, particularly during slow welding speeds, which provides higher heat inputs, leads to the formation of single and complex carbides ($Cr_{23}C_6$ - $Fe_{23}C_6$ - $M_{23}C_6$ - M_7C_3), which result in increasing the hardness in the bead region and in the near zone to the melting interface in the HAZ [18,19,20]. Furthermore, it was recorded a clear hardness drop, in both sides of the joint, relative to the hardness of the corresponding base plates, in the HAZ. This drop of hardness can be explained by the effect of temperature, on the previously deformed grain structure of the used plates, which were previously obtained by rolling. In fact, the temperature in these regions was relatively low, under the critical temperature of transformations, but enough to cause the recrystallization and grain growth of the structure, in these regions. We can note, also, that the amplitude of this drop is more pronounced in the low carbon steel side.

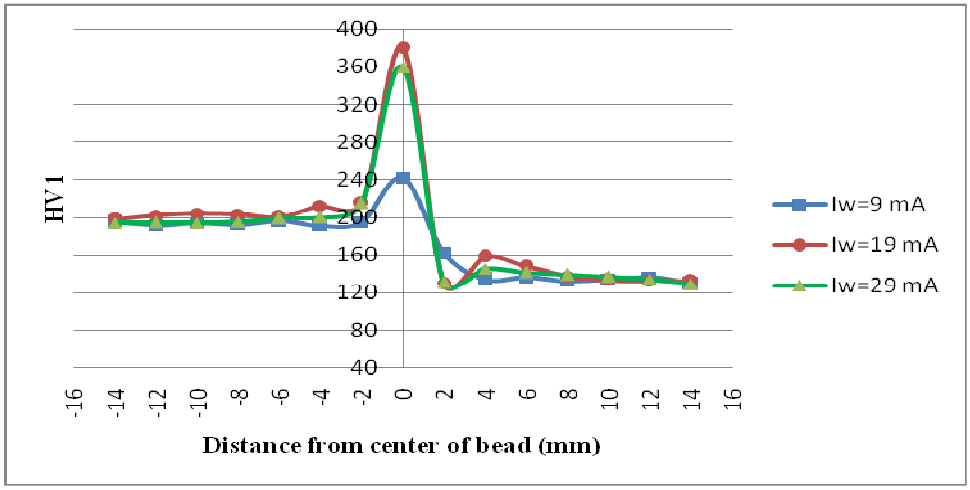

Fig. 20. The hardness distribution, along a line, from the stainless steel side of the welded plates, through the heat affected zones and formed bead, to the low carbon steel side of the joint under different welding current and constant I_f=875mA, and v=8mm/s.

CONCLUSION

1. Welding current and welding speed are considered the predominant welding parameters controlling the heat input to the welded joint and consequently the obtained structure and quality after solidification of the bead.

2. The optimum welding parameters, for welding dissimilar joints of AISI 304 stainless steel and AISI 1020 low carbon steel plates, having 5 mm thickness, are I_w=19 mA, I_f=875 mA, and v=8 mm/s. These parameters secure the highest strength, ductility, and toughness.

3. All tensile failures of the joints welded by the prescribed welding parameters took place in the AISI 1020 low carbon steel base metal, characterize by dimpled mode ductile fracture. Reducing the welding current to 9 mA, and keeping the other parameters constant, on the same dissimilar joint, the quality of the joint was reduced. Consequently, the fracture took place in the bead manifested a combined ductile and brittle fracture modes.

4. Ductility of the welded joint monotonically decreases by increasing both welding speed and focusing current.

5. Higher values of the impact toughness obtained when the hummer strikes against the root of the bead, where the joint acts as non-notched impact specimen. When hummer strikes against the face of the bead, the values of toughness is reduced to about half of the corresponding values obtained when hummer strikes against the face of the bead. The maximum values of impact toughness, in both directions of hummer strike relative to the bead were obtained at an optimum welding current of I_w=19 mA.

6. A peak of hardness was obtained in the center of the bead due to the diffusion process and formation of single and complex carbides. Hardness drops, in both sides of the joint, through the HAZ. Some regions in HAZ were subjected to softening by the recrystallization effect of the initial deformed plates structure.

REFERENCES

[1] Sindo Kou, ”Welding metallurgy”, Wiley, 2003.
[2] O.P. Khanna, “Welding Technology”, Dhanpat Rai Publications Ltd., 2006.
[3] W. Robbert, Jr. Messler, “ Joining of Materials and Structures”, ELSEVIER, 2003.
[4] R.S. Parmar, “Welding engineering and technology”, New Delhi: Khanna Publishers, 2003.
[5] David Leroy Olson, “Welding, Brazing, and Soldering”, Vol.6, ASM international, 1993.
[6] J. R. Davis, “Stainless Steels”, ASM International, Materials Park, Ohio, 1996.
[7] C. John, Lippold, and J. Kotecki Damian” Welding Metallurgy and Weldability of Stainless Steel”, Wiley, 2005.
[8] N. Yilbas, A.F.M. Arif, B.J. Abdul Aleem,” Laser welding of low carbon steel and thermal stress analysis”, Optics & Laser Technology, 42, (760–768), 2010.
[9] S. P. Tewari, “Effect of welding parameters on the weldability of material”, Inter. Jour. of Eng. Sci. and Tech., India vol. 2(4), (512-516), 2010.

[10] N. Arivazhagan, Surendra Singh, Satya Prakash, G.M. Reddy," Investigation on AISI 304 austenitic stainless steel to AISI 4140 low alloy steel dissimilar joints by gas tungsten arc, electron beam and friction welding", Mat. and Design, 32, (3036-3050), 2011.

[11] I. Hajiannia, M. Shamanian, M. Kasiri, "Microstructure and mechanical properties of AISI 347 stainless steel/A335 low alloy steel dissimilar joint produced by gas tungsten arc welding", Mat. and Design, 50, (566-573), 2013.

[12] Zhang Bing-gang, Wang Ting, Dyan Xiao-hui, "Temperature and stress fields in electron beam welded Ti-15-3 alloy to 304 stainless steel joint with copper interlayer sheet", Trans. Nonferrous Met. Soc., China 22,(398-403), 2012.

[13] L. Grecu, G. Demian," The Influence of welding parameters on temperature distribution in case of EBW", DAAAM inter. Scien. Book, 5, (035-044), 2009.

[14] Subodh Kumar, A.S. Shahi," Effect of heat input on the microstructure and mechanical properties of gas tungsten arc welded AISI 304 stainless steel joints", Mat. and Design,32, (3617-3623), 2011.

[15] Jun Yan, MingGao , Xiaoyan Zeng, " Study on microstructure and mechanical properties of 304 stainless steel joints by TIG, laser, and laser-TIG hybrid welding", Optics and Lasers in Eng., 48, (512–517), 2010.

[16] Carosena Meola, Antonino Squillace," Analysis of stainless steel welded joints: a comparison between destructive and non destructive techniques", Journal of Mat. Processing Tech., 155–156, (1893–1899), 2004.

[17] S. Murugan, Sanjai K. Rai, " Temperature distribution and residual stress due to multi-pass welding in type 304 stainless steel and low carbon steel weld pads", Inter. Jour. of pressure vessels and piping, 78, (307-317), 2001.

[18] T.Mohandas, G. Madhusudan Reddy and B. Satish Kumar," Heat-affected zone softening in high-strength low-alloy steels", Jour. of Mat. Processing Tech., Vol. 88, (284-294), 1999.

[19] M. Gokul Ananth, B.Sathish Babu," Experimental Investigations on Electron Beam Welding of Austenetic /Ferritic Stainless Steel for Space Applications", Inter. Jour. of Research in Mech. Eng. & Tech., IJRMET, Vol. 3, 2013.

[20] Andrzej Służalec," Theory of Thermo-mechanical Processes in Welding", Springer, 2005.